Sarah B. Duckworth*, Xavier Gaona*, Alexander Baumann, Kathy Dardenne, Jörg Rothe, Dieter Schild, Marcus Altmaier and Horst Geckeis

Impact of sulfate on the solubility of Tc(IV) in acidic to hyperalkaline aqueous reducing systems

https://doi.org/10.1515/ract-2021-1044
Received April 13, 2021; accepted July 11, 2021;
published online August 13, 2021

Abstract: The solubility of ^{99}Tc(IV) was investigated from undersaturation conditions in NaCl–Na_2SO_4 (0.3 M ≤ I ≤ 5.0 M), $MgCl_2$–$MgSO_4$ (I = 13.5 M) and $CaCl_2$–$CaSO_4$ (I = 13.5 M) systems with 0.001 M ≤ $[SO_4^{2-}]_{tot}$ ≤ 1.0 M and 1 ≤ pH_m ≤ 12 (with pH_m = –log[H^+], in molal units). Reducing conditions were set by either Sn(II) or Fe(0). Special efforts were dedicated to accurately characterize the correction factors A_m required for the determination of pH_m from the experimentally measured pH values in the mixed salt systems investigated, with $pH_m = pH_{exp} + A_m$. The combination of (pe + pH_m) measurements with *Pourbaix* diagrams of Tc suggests that technetium is present in its +IV redox state. This hypothesis is confirmed by XANES, which unambiguously shows the predominance of Tc(IV) both in the aqueous and solid phases of selected solubility samples. XRD and SEM–EDS support the amorphous character of the solid phase controlling the solubility of Tc(IV). EXAFS data confirm the predominance of TcO_2(am, hyd) at pH_m > 1.5, whereas the formation of a Tc(IV)–O–Cl solid phase is hinted at lower pH_m values in concentrated NaCl–Na_2SO_4 systems with ≈5 M NaCl. Solubility data collected in sulfate-containing systems are generally in good agreement with previous solubility studies conducted in sulfate-free NaCl, $MgCl_2$ and $CaCl_2$ solutions of analogous ionic strength. Although the complexation of Tc(IV) with sulfate cannot be completely ruled out, these results strongly support that, if occurring, complexation must be weak and has no significant impact on the solubility of Tc(IV) in dilute up to highly saline media. Solubility upper-limits determined in this work can be used for source term estimations including the effect of sulfate in a variety of geochemical conditions relevant in the context of nuclear waste disposal.

Keywords: complexation; solubility; sulfate; technetium; thermodynamics.

***Corresponding authors: Sarah B. Duckworth and Xavier Gaona**, Institute for Nuclear Waste Disposal, Karlsruhe Institute of Technology, P.O. Box 3640, 76021 Karlsruhe, Germany, E-mail: sarah.duckworth@kit.edu (S. B. Duckworth), Xavier.gaona@kit.edu (X. Gaona)
Alexander Baumann, Kathy Dardenne, Jörg Rothe, Dieter Schild, Marcus Altmaier and Horst Geckeis, Institute for Nuclear Waste Disposal, Karlsruhe Institute of Technology, P.O. Box 3640, 76021 Karlsruhe, Germany

1 Introduction

^{99}Tc is a β-emitting fission product forming in nuclear reactors through the fission of ^{235}U and ^{239}Pu. ^{99}Tc is of special relevance in the context of long-term safety assessment of repositories for nuclear waste due to its long half-life ($t_{1/2}$ ^{99}Tc = 2.13 x 10^5 a), large inventory in spent nuclear fuel and of its remarkably different chemical behavior in the predominant oxidation states +IV and +VII.

Under oxidizing to weakly reducing conditions, Tc is found as mobile TcO_4^- in aqueous media. Under the very reducing conditions expected to develop after closure in most underground repository concepts where Tc(IV) is expected to predominate, the aquatic chemistry of technetium will be controlled in the form of the sparingly soluble TcO_2(am, hyd).

Sulfate is an abundant component in many natural groundwater and one of the most relevant anions (besides chloride) in brines eventually forming in salt-rock formations, where sulfate concentrations of up to 0.2 M can be expected [1–4]. Corrosion of cementitious materials in $MgCl_2$-dominated brines may lead to high $CaCl_2$ concentrations (≥2 M) and highly alkaline pH_m (≈12) conditions [1, 5]. In such systems, sulfate concentration in solution is mainly controlled by the solubility of gypsum ($CaSO_4 \cdot 2H_2O$), which defines significantly lower sulfate concentrations (≤0.001 M). Although sulfate is a relatively weak ligand, the high concentrations possibly expected in certain repository settings may potentially lead to the complexation of radionuclides, eventually enhancing solubility and decreasing sorption.

Besides hydrolysis, only a limited number of experimental studies have been conducted to evaluate the complexation of Tc with inorganic ligands, most of them dedicated to chloride and carbonate [6–11]. A few studies investigated the interaction of Tc(IV) with sulfate, in all

cases focusing on acidic conditions that are of limited or no relevance in the context of nuclear waste disposal. In view of these experimental efforts, the thermodynamic data reported for this system is very sparse and the Thermochemical Database Project of the Nuclear Energy Agency (NEA–TDB) does not select any data for this system [12–14]. Spitsyn et al. reported the formation of a brownish Tc(IV)-sulfate complex in the electrolytic reduction of Tc(VII) in 0.71 M sulfuric acid [15]. Based on the combination of electrophoresis and UV–vis spectroscopy data as a function of pH, the authors proposed the stoichiometry $Tc(OH)_2(SO_4)_2^{2-}$ for this complex. Ianovici et al. investigated the photochemical decomposition of $TcCl_6^{2-}$ in three different acids (1 M HCl, 1 M $HClO_4$, 1 M H_2SO_4) using a combination of electrophoretic separation and spectroscopic methods [16]. At long irradiation times, the authors reported the predominance of cationic species in HCl and TcO_4^- in $HClO_4$, whereas a neutral species was found to prevail in H_2SO_4. The dissolution of TcO_2(s) in H_2SO_4 led to the formation of a similar species as confirmed by UV–vis spectroscopy. This uncharged species was considered to be either a sulfato- or colloidal species of Tc(IV). These findings are in disagreement with the formation of the charged species reported by Spitsyn et al. In a XAS study with Tc(IV) in mixed sulfate/chloride and sulfate media, Vichot et al. were able to fit only Tc–O and Tc–Tc backscatters but did not report a Tc–S interaction [17]. The authors concluded that Tc(IV) oligomeric species were formed, and that these were independent of the background electrolyte/anion present [17]. An extended work by the same authors using UV–vis spectroscopy suggested the formation of a trimeric moiety ($Tc_3O_4^{4+}$), which led to the neutral complex $Tc_3O_4(SO_4)_2$(aq) in acidic solutions with $0 \le pH \le 1.5$ and $[SO_4^{2-}]_{free} \ge 0.1$ M (with total sulfate concentrations up to 2.1 M) [18]. A recent study by Parker et al. investigated the complexation of Tc(IV) with sulfate by solvent extraction with HDEHP and TOPO. Experiments were performed at constant ionic strength (I = 1.0 M) in NaCl–Na_2SO_4 solutions with 0.075 M ≤ $[Na_2SO_4]$ ≤ 0.25 M and pcH = (1.51 ± 0.05) (with pcH = –log $[H^+]$). The values of pcH were determined from the experimentally measured pH (pHr in the paper) and using an empirical correction equation determined by the authors in 1.0 M NaCl. The application of this empirical equation to mixed NaCl–Na_2SO_4 systems can result in large systematic deviations in the values of pcH (see Section 3.3). Based on their solvent extraction data, the authors proposed the formation of the complex $TcO(OH)SO_4^-$ with a log β' = (1.13 ± 0.04). Note that the definition of this species is bound to the underlying hydrolysis model used by the authors, which assumes the predominance of $TcO(OH)^+$ at this pcH [19].

In this context, this study focuses on the impact of sulfate on the solubility of Tc(IV) under acidic to hyperalkaline pH conditions, covering dilute to concentrated salt systems as those expected in different repository concepts for waste disposal. Solubility data are complemented with extensive solid phase characterization methods and advanced spectroscopic techniques to fill in some of the literature gaps discussed above.

2 Thermodynamic background and sulfate complexation

Tc(IV) is characterized by a strong hydrolysis and a very low solubility defined by the amorphous hydrous oxide TcO_2(am, hyd). The strong hydrolysis leads to an amphoteric behavior with the predominance of cationic and anionic species under acidic and hyperalkaline pH conditions, respectively. In our previous experimental studies dedicated to the solubility and hydrolysis of Tc(IV), we derived comprehensive chemical, thermodynamic and (SIT, Pitzer) activity models for the system Tc^{4+}–Na^+–K^+–Ca^{2+}–Mg^{2+}–H^+–Cl^-–OH^-–H_2O(l) [9, 10]. In line with other spectroscopic evidence available in the literature, the predominance of a trimeric species ($Tc_3O_5^{2+}$) in acidic conditions was reported [17, 18]. This model is able to accurately predict solubility phenomena in dilute to concentrated NaCl, KCl, $MgCl_2$ and $CaCl_2$ solutions with $2 \le pH_m \le 14$, and thus provides the baseline to evaluate the effect of different complexing ligands in these background electrolyte systems.

In the concept of Hard and Soft Acid Bases (HSAB), sulfate is often considered as a borderline base. Despite its charge –2, sulfate is a relatively weak ligand because of the delocalization of the electron density within its tetrahedral structure. The strength of the complexes forming between hard cations (as Tc(IV)) and different ligands can be qualitatively classified as follows [20]:

$$PO_4^{3-} > CO_3^{2-} > OH^- > SiO(OH)_3^- > HPO_4^{2-} > F^- > SO_4^{2-} > H_2PO_4^- > H_3PO_4 > NO_3^- > Cl^-$$

According to the classification above, the sulfate complexes of Tc(IV) should be significantly weaker than hydrolysis, especially at high pH where high hydroxide concentrations prevail. Nonetheless, in the presence of high concentrations of sulfate in solution, complexation may outcompete hydrolysis, eventually resulting in an increase of Tc(IV) solubility. Although the corresponding thermodynamic data are not available for the Tc(IV)

system, Table 1 provides some insights in the strength of sulfate complexes with respect to hydrolysis for other M(IV) of relevance in the context of nuclear waste disposal, namely Th(IV), U(IV), Np(IV), Pu(IV) and Zr(IV). Table 1 gives also information on the corresponding ionic radii of the M^{4+} cations, which gives insight of the "hardness" of the cation as Lewis acid.

Table 1 shows the very large differences (between 5.3 and 9.7 $\log_{10}$-units) existing between the stability of the first hydrolysis species and sulfate complexes. This implies that a sulfate excess of ~10^5 to ~10^{10} with respect to the hydroxide concentration is required to outcompete hydrolysis considering the chemical reaction (1):

$$M^{IV}OH^{3+} + SO_4^{2-} \Leftrightarrow M^{IV}SO_4^{2+} + OH^- \quad (1)$$

$$\log K^\circ\ (1) = \log \beta^\circ\left(M^{IV}SO_4^{2+}\right) - \log \beta^\circ\left(M^{IV}OH^{3+}\right)$$

The cation Tc^{4+} is smaller than Zr^{4+} ($r_{Tc}{}^{4+}$ = 0.645 Å, with CN = 6), which accordingly results in an enhanced hydrolysis with respect to all other tetravalent metals in Table 1. Indeed, Tc^{4+} readily hydrolyses in very acidic conditions, and the cation TcO^{2+} (or likely $Tc_3O_5{}^{2+}$, as described in Yalçıntaş et al.) is the one controlling the solution chemistry of Tc(IV) under such conditions [10]. This characteristic feature makes it difficult to predict the competition between sulfate and hydroxide for Tc(IV) on the basis of the analogy with other M(IV).

3 Experimental

3.1 Chemicals

Sodium chloride (NaCl, p.a.), sodium sulfate anhydrous (Na_2SO_4, p.a.), sodium dithionite anhydrous ($Na_2S_2O_4$, ≥87%), calcium chloride dihydrate ($CaCl_2 \cdot 2H_2O$, p.a.), magnesium chloride hexahydrate ($MgCl_2 \cdot 6H_2O$, p.a.), magnesium sulfate heptahydrate ($MgSO_4 \cdot 7H_2O$, p.a.), chloroform ($CHCl_3$, p.a.) and iron powder (grading 10 µm, p.a.) were obtained from Merck. 2-(N-morpholino)ethanesulfonic acid ($C_6H_{13}NO_4S$, MES), 1,4-piperazinediethanesulfonic acid disodium salt ($C_8H_{17}N_2Na_2O_6S_2$, PIPES) and tin(II) chloride ($SnCl_2$, 98%) were purchased from Sigma-Aldrich. Ethanol (99.9%) was obtained from VWR Chemicals.

All sample solutions were prepared using purified water Millipore Milli-Q Advantage A10 (18.2 MΩ cm at 25 °C, 4 ppb TOC) with Millipore Millipak® 40 filter 0.22 µm, which was purged with Ar for 1 h to remove traces of oxygen before use. Handling, preparation and storage of all samples were performed in an Ar glovebox with <3 ppm O_2, <1 ppm H_2O at (22 ± 2) °C.

The Tc(IV) stock solution used in all the experiments was prepared from a chemically well characterized ^{99}Tc stock solution (0.6 M $NaTcO_4$). The Tc(VII) stock solution was reduced electrochemically in 1.0 M HCl, and subsequently precipitated as TcO_2(s) under alkaline and reducing conditions ($Na_2S_2O_4$, pH_m > 12.5) following the procedure previously described by Yalçıntaş, Baumann and co-workers [8, 10]. The obtained solid phase was stored as suspension in a Kautex container (LDPE) at ambient temperature inside the glovebox. No special precaution were taken to exclude light. The solid phase was aged for at least three months before use in solubility experiments.

To adjust the pH of the samples, sodium hydroxide (NaOH, Titrisol® Merck), hydrochloric acid (HCl, Titrisol® Merck), as well as magnesium hydroxide ($Mg(OH)_2$, ≥99%; Fluka) and freshly prepared calcium hydroxide were used. Calcium hydroxide ($Ca(OH)_2$) was precipitated by slow titration of a 2.0 M $CaCl_2$ solution with 1.0 M NaOH. The resulting solid was washed five times with Milli-Q water before use.

For the 1 M NaOH (Titrisol) used in this work, the carbonate concentration was determined in a previous study as $(3.1 \pm 0.2) \times 10^{-5}$ M [25]. Those impurities are considered to have a negligible impact in the context of this study.

Liquid scintillation counting (LSC) was performed with LSC-cocktail Ultima Gold™ XR from Perkin Elmer.

Table 1: Equilibrium constants for the formation of MOH^{3+} and $MSO_4{}^{2+}$ (with M = Th, U, Np, Pu and Zr) according to the equilibrium reactions $M^{4+} + L^{n-} \Leftrightarrow ML^{(4-n)}$ (with $L^{n-} = OH^-$ and $SO_4{}^{2-}$). Values of ionic radii as reported in Neck and Kim and Shannon for the oxidation state +IV with coordination number (CN) of 9 [21, 22].

	Ionic radii [Å]	MOH^{3+} $\log \beta^\circ$	$MSO_4{}^{2+}$ $\log \beta^\circ$	Reference
Th^{4+}	(1.08 ± 0.02)	(11.50 ± 0.50)	(6.17 ± 0.32)	[23]
U^{4+}	(1.04 ± 0.02)	(13.46 ± 0.06)	(6.58 ± 0.19)	[12]
Np^{4+}	(1.02 ± 0.02)	(14.55 ± 0.20)	(4.87 ± 0.15)	[12]
Pu^{4+}	(1.01 ± 0.02)	(14.60 ± 0.20)	(4.91 ± 0.22)	[12]
Zr^{4+}	0.89 [22]	(14.32 ± 0.22)	(7.04 ± 0.09)	[24]

3.2 pH_m and E_h measurements

The proton concentration ($pH_m = -\log[H^+]$, $[H^+]$ in molal units (m = mol kg_w^{-1})) was measured using a ROSS combination pH electrode (Thermo Scientific, Orion™) calibrated against standard buffer solutions (pH = 2–10, Merck). In aqueous solutions with ionic strength $I_m \geq 0.1$ m, the measured pH value (pH_{exp}) is an operational apparent value related to the molal proton concentration $[H^+]$ by $pH_m = pH_{exp} + A_m$. The empirical correction factor A_m entails both the liquid junction potential of the electrode as well as the activity coefficient of $[H^+]$. A_m values for chloride systems are well known and have been previously reported in the literature for NaCl, $MgCl_2$ and $CaCl_2$ systems [26, 27]. A_m values for the sulfate and mixed chloride-sulfate systems have been determined in this work as reported in Section 3.3.

In $MgCl_2$ and $CaCl_2$ solutions, the highest pH_m (pH_{max}) is defined by the precipitation of the hydroxides $Mg(OH)_2$(s) and $Ca(OH)_2$(s) (or corresponding oxychlorides at Ca or Mg concentrations above ≈2 m), which buffer the pH_m at ≈9 and ≈12, respectively [10, 26].

E_h measurements were conducted using a Pt combination electrode (Metrohm) with Ag/AgCl as a reference system. The measured redox potentials were converted to E_h *versus* SHE (standard hydrogen electrode) by correcting for the potential of the Ag/AgCl reference electrode (+207 mV for 3 M KCl at 25 °C). All samples measured were stirred continuously for 25 min during the measurement. In analogy to

the pH value, the apparent electron activity (pe = $-\log a_{e^-}$) was calculated from pe = 16.9 E_h [V], according to the equation $E_h = \frac{RT \ln(10)}{F}$ pe.

The accuracy of the redox electrode was tested with a standard redox buffer solution (+220 mV *vs.* Ag/AgCl, Schott) and provided readings within ±10 mV of the certified value.

3.3 Determination of A_m values

A_m-values are usually determined in acidic conditions using a set of reference solutions with known H^+ concentration [9, 26–29]. In background electrolyte solutions without any component consuming protons, the A_m-value can be directly determined from the difference between the initial H^+ concentration (corresponding to the free H^+ concentration in solution) and the experimental pH (pH_{exp}) measured with the glass electrode. In sulfate systems however, the formation of HSO_4^- in acidic conditions ($pK°_{a2} = 1.98 \pm 0.05$) decreases the initial free proton concentration and thus prevents this method of straightforward quantification of A_m-values. For this reason, the determination of A_m-values of sulfate systems in acidic conditions requires the use of an activity model for the calculation of $[HSO_4^-]_{free}$, $[SO_4^{2-}]_{free}$ and $[H^+]_{free}$ (see for instance Rai et al.) [29].

A different approach was preferred in the present work, involving the use of alkaline solutions that avoid the formation of the bisulfate species. This approach was used for the quantification of the A_m-values in the NaCl–Na_2SO_4 system. Due to the limitations in pH_m imposed by the precipitation of $Mg(OH)_2$(s) (with $pH_{max} \approx 9$), this approach could not be used for the $MgCl_2$–$MgSO_4$ system, and the A_m-values reported for pure $MgCl_2$ systems were used instead. The concentration of sulfate in the investigated $CaCl_2$–$CaSO_4$ systems is very low (0.001 M), and thus A_m-values reported for the pure $CaCl_2$ systems were used for the calculation of pH_m from pH_{exp}. A set of reference solutions with known hydroxide concentrations (1.00×10^{-2}–3.13×10^{-4} M) was prepared for different Na_2SO_4 and NaCl–Na_2SO_4 systems (see Table 2). The free H^+ concentration in each sample (as pH_m) was calculated from the hydroxide concentration and using the values of $\log K'_w$ calculated with the Pitzer thermodynamic database THEREDA and the software PhreeqC [30–32]. A_m-values were calculated as $A_m = pH_m - pH_{exp}$.

A more detailed procedure for the determination of Am factors including the measured pH value of each sample is given in Tables SM-1 and SM-2 of the Supplementary Material.

3.4 Solubility experiments

Batch solubility experiments were performed from undersaturation conditions using the TcO_2(am, hyd) solid prepared in this work and aged for three months. Solubility samples in NaCl–Na_2SO_4 (I = 0.3, 1.0 and 5.0 M, $1.0 \le pH_m \le 12.3$, 37 samples), $MgCl_2$–$MgSO_4$ (I = 13.5 M, $6.7 \le pH_m \le 9.3$, 16 samples, of which five remained inactive for comparison reasons), and $CaCl_2$–$CaSO_4$ (I = 13.5 M, $5.8 \le pH_m \le 12.0$, three samples) solutions were prepared in polyethylene vials with 25 mL matrix solution and ≈2 mg of Tc(IV) solid per sample. HCl–NaCl and NaOH–NaCl solutions of appropriate ionic strength were used to adjust the pH_m values in the NaCl–Na_2SO_4 system. In the $MgCl_2$–$MgSO_4$ system, the pH_m values were set using HCl–$MgCl_2$ solutions of appropriate ionic strength and solid $Mg(OH)_2$(s). MES (0.33–1.33 mM, using a stock solution of 1.0 M) and PIPES (10 mM, using a stock solution of 0.5 M) were used to buffer the solutions at pH_m = 7 and 8, respectively. HCl–$CaCl_2$, PIPES buffer (1.66 mM, using a stock solution of 0.5 M) and freshly precipitated $Ca(OH)_2$(s) were used to adjust the pH_m in the $CaCl_2$–$CaSO_4$ system at ≈5, 9 and 12. The highest sulfate concentrations considered in the $MgCl_2$–$MgSO_4$ and $CaCl_2$–$CaSO_4$ system were selected to remain below the solubility of the corresponding sulfate salts [33, 34].

In order to maintain reducing conditions and to avoid oxidation of Tc(IV), 2 mM of Sn(II) or ≈7 mg Fe(0) powder were added to each of the samples. Previous studies by Kobayashi et al., Yalçıntaş et al. and Baumann et al., have shown that very reducing conditions could be maintained over a longer time frame with Sn(II) and Fe(0) present in solution [9–11, 35]. Possible formation of Sn-or Fe doped Tc solids were neither observed within this study nor in other studies performed previously and are therefore considered to be unlikely. In addition, SEM-EDX measurements could not detect any such species. Sn(II) shows an amphoteric behavior and forms the sparingly soluble $Sn(OH)_2$(s) (or $Sn_6O_4(OH)_4$(s), see Gamsjäger et al.) [36]. For this reason, in most of the samples buffered with Sn(II) this reducing chemical was present as a solid. Commercial Fe(0) powder was washed with an acidic solution (pH ≈ 2) for 30 min to remove any oxidized surface coating. Samples were equilibrated for 14 days in an Ar-glovebox, and pH_m and E_h values monitored until confirming that stable pH values and the necessary reducing conditions were attained. Approximately 2 mg of Tc(IV) solid phase were washed three times with 1 mL of the respective matrix solution and then added to 25 mL of the same matrix solution in a screw cap vial (Nalgene™, Thermo Scientific). Technetium concentration after 10 kD ultrafiltration, pH_m and E_h were measured at regular time intervals for up to 428 days. Previous test experiments performed with Th(IV) and Tc(IV) (see Altmaier et al. or Yalçıntaş et al.) confirmed that the sorption of tetravalent metals in trace concentrations is negligible for this specific type of filter (Nanosep®, Pall Life Science). No filter clogging was observed throughout the experiment [11, 37].

The Tc concentration was measured by LSC (liquid scintillation counting). Therefore 500 µL of supernatant fluid were removed from the solubility sample and centrifuged in polypropylene tubes with 10 kD filters (Omega™, 2–3 nm cut-off, Nanosep®, Pall Life Science) for 5 min (13,500 rpm, 12,225 *g*) to separate possible colloids or suspended solid phase particles. Four hundred microliter of the filtrate were then pipetted into 600 µL of HCl (1.0 M), and 600 µL of the resulting solution were added to 10 mL of LSC cocktail in a screw-cap vial (PP, 20 mL, Zinsser Analytic). The samples were measured for 30 min each using a LKB Wallac 1220 Quantulus (Perkin-Elmer) liquid scintillation counter. A detection limit of 9×10^{-10} M was calculated as threefold the standard deviation of five inactive blanks.

A summary of all the solubility samples investigated in this work is provided in Table 3.

Table 2: Sample preparation scheme used for the determination of A_m-factors in Na_2SO_4 and NaCl–Na_2SO_4 solutions investigated in this work.

I [M]	[NaCl]/[Na_2SO_4] [M]			
0.30	0.27/0.01	0.00/0.10		
1.00	0.97/0.01	0.70/0.10	0.00/0.333	
2.50	0.00/0.833			
5.00	4.7/0.10	3.50/0.50	2.00/1.00	0.00/1.67

Table 3: Summary of experimental conditions used in the solubility experiments with TcO_2(am, hyd). All experiments were conducted in the presence of Sn(II) as reducing agent, except in a number of selected samples for which Fe(0) was used instead. The inactive samples (no Tc added) used for comparison purposes.

I [M]	[NaCl]/[Na_2SO_4] [M] (number of samples)				pH_m-range
	Sn(II)			Fe(0)	
0.3	0.27/0.01 (5)	0.00/0.10 (5)		0.27/0.01 (1)	1.0–12.3
1	0.97/0.01 (5)	0.70/0.10 (6)		0.97/0.01 (1)	
5	4.7/0.10 (6)	3.50/0.50 (6)	2.00/1.00 (1)	4.7/0.10 (1)	
	[$MgCl_2$]/[$MgSO_4$] [M] (number of samples)				
13.5	Sn(II)		Fe(0)		
	4.49/0.01 (3)		4.49/0.01 (1)		
	4.37/0.10 (3)				
	4.10/0.30 (3)		4.10/0.30 (1)		
	Inactive samples without Tc				6.7–9.3
	Sn(II)		Fe(0)		
	4.49/0.01 (1)		4.49/0.01 (1)		
	4.37/0.10 (1)				
	4.10/0.30 (1)		4.10/0.30 (1)		
	[$CaCl_2$]/[$CaSO_4$] [M] (number of samples)				
	Sn(II)				
13.5	4.499/0.001 (3)				5.8–12.0

3.5 Solid phase characterization

After attaining equilibrium conditions, solid phases of four selected solubility samples were characterized by X-ray diffraction (XRD), scanning electron microscope energy dispersive spectrometry (SEM-EDS) and quantitative chemical analysis:

(i) 0.1 M Na_2SO_4 (pH_m = 11.4),
(ii) 0.5 M Na_2SO_4 + 3.5 M NaCl (pH_m = 11.8),
(iii) 1.0 M Na_2SO_4 + 2.0 M NaCl (pH_m = 3.5), and
(iv) 0.3 M $MgSO_4$ + 4.1 M $MgCl_2$ (pH_m = 9.3).

For each of the investigated samples, an aliquot of approximately 1 mg of Tc solid-phase was washed five times with 1 mL of ethanol inside an Ar-glovebox. This washing procedure aimed at a complete removal of the salt-containing matrix, which can interfere in the characterization of the Tc solid. After the last washing step, the solid phase was suspended in ≈30 µL of ethanol and transferred to an airtight, capped silicon single crystal sample holder (Dome, Bruker). After the evaporation of ethanol, the sample was taken out of the glovebox and XRD data was collected on a Bruker AXS D Advance X-ray powder diffractometer. Measurements were performed at angles 2θ = 5–60° with incremental steps of 0.02–0.04° and a measurement time of 3–8 s per increment, while the sample was rotating at 15 rpm. The resulting diffraction patterns were compared with powder diffraction files (PDF) provided by the JCPDS-ICDD database [38]. After the measurement, the solid phase was dissolved in 1–2 mL of 2% HNO_3 and the solution was used for quantitative chemical analysis (Tc concentration by LSC measurements and Na by inductively coupled plasma-optical emission spectroscopy, ICP-OES).

A second fraction of the washed solid phase (*ca.* 20 µg) was characterized by SEM–EDS using a Quanta 650 FEG apparatus equipped with a Noran EDS unit.

3.6 XANES and EXAFS measurements

Technetium K-edge X-ray absorption near-edge structure (XANES) and Extended X-ray Absorption Fine Structure (EXAFS) spectra of selected samples were collected at the INE-Beamline at the KIT synchrotron source (KARA storage ring, formerly ANKA, KIT Campus North, in Karlsruhe (Germany)), using the conventional fluorescence yield XAS setup at the INE-Beamline [39, 40]. The Tc K_α-line was detected by combining the signal of a 4-pixel and a single-pixel silicon drift (Vortex) detector (Hitachi, USA), using an Ar-filled ionization chamber (Poikat, Germany) at ambient pressure as I_0 monitor. The double crystal monochromator was equipped with a pair of Ge<422> crystals. The energy scale was calibrated by assigning the first inflection point in the rising K-edge absorption of a Mo metal foil (20 µm) to the 1s-energy (E_{1s} (Mo^0): 20.0 keV).

For all investigated samples, about 350 µL of the suspension was transferred into a 400 µL polyethylene vial under Ar atmosphere and centrifuged for 7 min at 5900 *g* to compact the solid at the bottom of the vial and have a clear phase separation for XAFS measurements. The vials were mounted in a gas-tight cell with windows of Kapton® film. During the measurements the cell was flushed continuously with helium.

4 Results and discussion

4.1 Determination of A_m values for the correction of pH_{exp}

Empiric correction factors to convert the directly measured pH_{exp} values into molal proton concentrations pH_m, A_m values, were determined experimentally for aqueous Na_2SO_4 and NaCl–Na_2SO_4 solutions. Figure 1 shows the A_m values obtained for pure Na_2SO_4 solutions as described in Section 3.3. The figure includes also A_m values reported for the same system (determined also in alkaline conditions) by Rai and co-workers [29]. A_m values determined elsewhere in NaCl [26], $NaNO_3$ [28], $MgCl_2$ [26] and $CaCl_2$ [27] are also added to the figure for comparative purposes.

A_m values determined for pure Na_2SO_4 systems follow a U-shape and range between −0.45 and −0.24 for the investigated salt concentrations (0.1 m ≤ [Na_2SO_4] ≤ 1.87 m). On the contrary, A_m values reported for NaCl, $NaNO_3$, $MgCl_2$ and $CaCl_2$ linearly increase with increasing salt concentration. As described in Section 3.3, A_m values for a given background electrolyte and background electrolyte concentration are mostly contributed by two terms, namely the activity coefficient of H^+ and the liquid junction potential of the electrode for the given media. Figure SM-1 in Supplementary Material shows the activity coefficients of H^+ calculated for NaCl, $MgCl_2$, $CaCl_2$ and $NaNO_3$ (using SIT coefficients reported in NEA-TDB), or calculated in the present work for Na_2SO_4 [12]. Table SM-3 in Supplementary Material also summarizes the calculated values of log γ_{H^+} and the values of A_m determined in the present work for 0.1, 0.336, 0.851 and 1.754 m Na_2SO_4. Two main conclusions can be extracted from Figure SM-1 and Table SM-3: (i) the values of log γ_{H^+} in Na_2SO_4 behave very differently to all other salt systems considered in the comparison, and (ii) log γ_{H^+} is a very relevant contribution to A_m in the case of Na_2SO_4, accounting at least for half of the correction factor. The liquid junction potential results from differences in the mobility of the ions present in the reference internal solution (usually KCl) and the ions in the background electrolyte solution. The comparison of the relative mobility of Cl^- (1.04), NO_3^- (0.97), SO_4^{2-} (0.54) and HSO_4^- (0.71) (relative to K^+, calculated from diffusion coefficients reported by Vanysek) gives the additional confirmation of the different behaviour observed for the A_m values in sulfate systems [41, 42].

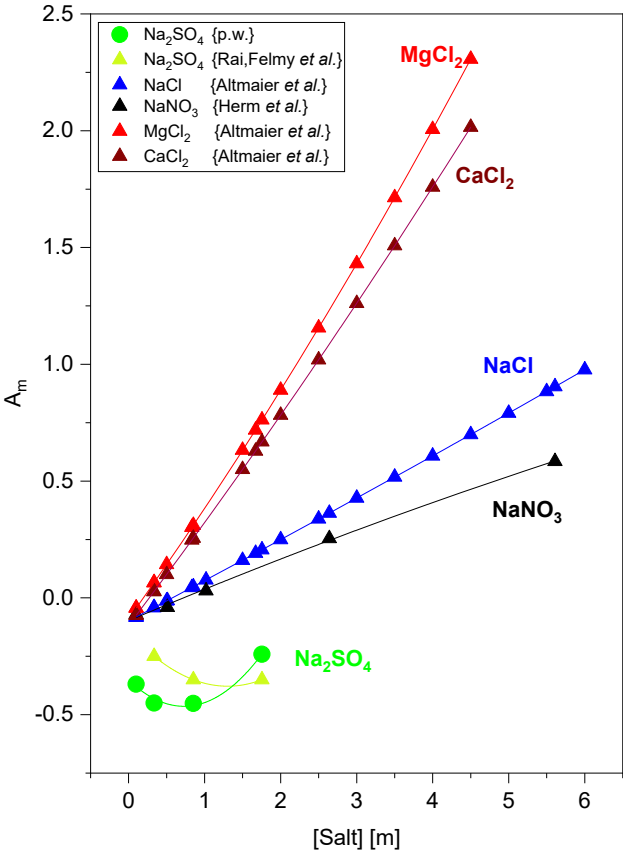

Figure 1: A_m values determined in the present work for pure aqueous Na_2SO_4 solutions (obtained in alkaline conditions) and reported in the literature for NaCl [26], $NaNO_3$ [28], Na_2SO_4 [29], $MgCl_2$ [26] and $CaCl_2$ [27].

Figure 1 shows also some discrepancies (≤0.2) between A_m values determined for the Na_2SO_4 system in the present work and in Rai et al. [29]. A closer look at the Pitzer parameters used in one case and the other for the calculation of the ion activities in the system Na^+–H^+–OH^-–HSO_4^-–SO_4^{2-}–H_2O(l) shows clear differences (see Table SM-2 in the Supplementary Material). This affects the calculation of log γ_{H^+} and log γ_{OH^-}, and can therefore partially explain the differences between the two sulfate-datasets included in Figure 1. A_m values determined in this work for pure Na_2SO_4 and mixed NaCl–Na_2SO_4 systems are summarized in Table 4.

The maximum pH_m (pH_{max}) in $MgCl_2$ solutions is buffered to ≈9 by the precipitation of $Mg(OH)_2$(cr), or $Mg_2(OH)_3Cl{\cdot}4H_2O$(cr) in solutions with [$MgCl_2$] ≥ 2 m [26]. Consequently, the approach used in the determination of A_m values for NaCl–Na_2SO_4 solutions under highly alkaline conditions cannot be applied to aqueous $MgCl_2$–$MgSO_4$ systems. Instead, A_m values for mixed $MgCl_2$–$MgSO_4$ solutions were calculated by using A_m values for the pure

Table 4: A_m values determined in the present work in alkaline conditions for NaCl–Na_2SO_4 systems of different ionic strength. Values in italics correspond to pure aqueous Na_2SO_4 systems.

Ionic strength [*m*]	[Na_2SO_4] [*m*]							
	No sulfate	**0.01**	**0.1**	**0.34**	**0.51**	**0.85**	**1.03**	**1.75**
0.3	−0.05	−0.24	*−0.37*					
1.0	0.08	−0.11	−0.18	*−0.45*				
2.55						*−0.45*		
5.2–5.5	0.9		0.86		0.71		0.41	*−0.24*

$MgCl_2$ system. This approach bears larger uncertainties than the experimental determination of A_m, although the impact is considered less relevant because of the relatively low sulfate concentrations (≤0.3 M) compared to the total chloride concentrations (≥4.1 M) in the investigated $MgCl_2$–$MgSO_4$ systems.

A_m values summarized in Table 4 for NaCl–Na_2SO_4 solutions are used in the following sections for the determination of pH_m values in Tc(IV) solubility experiments conducted in the same background electrolyte conditions. An uncertainty of ± 0.20 is assigned to pH_m values in NaCl–Na_2SO_4 solutions, which is estimated based on the differences observed between A_m values determined in the present work and in Rai et al. [29]. A slightly larger uncertainty ±0.25 is assigned to $MgCl_2$–$MgSO_4$ for the reasons indicated above. Note that these uncertainties are significantly larger than ±0.05 usually considered in standard determinations of pH_m, and reflect the additional uncertainties arising from the thermodynamic calculations involved in the determination of A_m values.

4.2 Pourbaix diagrams and experimental (pe + pH_m) measurements

Figures 2 and 3 show the Pourbaix diagrams of Tc calculated for the conditions of the investigated NaCl–Na_2SO_4, $MgCl_2$–$MgSO_4$ and $CaCl_2$–$CaSO_4$ systems. The figures include also (pe + pH_m) values measured for the Tc(IV) solubility samples in the presence of Sn(II) and Fe(0) as reducing systems. The colored lines in Figures 2 and 3 represent a 1:1 distribution of the redox couple Tc(VII)/Tc(IV) according to reaction (2):

$$TcO_4^- + 4H^+ + 3e^- \Leftrightarrow TcO_2 0.6H_2O\,(s) + 1.4\,H_2O\,(l) \quad (2)$$

$$\log {}^{*}K'_{VII-IVs}$$

The conditional constants $\log {}^{*}K'_{VII-IVs}$ are calculated using thermodynamic data and SIT coefficients reported by Yalçıntaş and co-workers [10, 11]. Solid and dashed colored lines correspond to the thermodynamic calculations performed for pure chloride systems of the same ionic strength.

Values of (pe + pH_m) in NaCl–Na_2SO_4, $MgCl_2$–$MgSO_4$ and $CaCl_2$–$CaSO_4$ solutions lie well below the calculated Tc(VII)/Tc(IV) redox borderline, therefore supporting the only presence of Tc(IV) in all investigated systems. Very similar (pe + pH_m) values are measured before and after the addition of Tc(IV) (data only available for $MgCl_2$–$MgSO_4$), thus indicating that the addition of Tc does not impact the overall redox conditions of the system, which are controlled either by Sn(II) or by Fe(0). The values of (pe + pH_m) measured for both redox buffers generally agree with previous investigations with Tc using both reducing chemicals [10, 11, 35]. One exception is the (pe + pH_m) value determined in a 4.7 M NaCl + 0.1 M Na_2SO_4 at pH_m = 12, which is significantly lower than analogous measurements reported by Yalçıntaş et al. in 5.0 M NaCl [11]. The passivation of Fe(0) under hyper alkaline conditions, very likely through the formation of magnetite, has been indeed reported in several publications [43, 44]. The absence of this effect in the present work might be related to the impact of sulfate on the solution chemistry of Fe.

4.3 Solid phase characterization

XRD patterns collected for selected Tc(IV) solid phases equilibrated in NaCl–Na_2SO_4 and $MgCl_2$–$MgSO_4$ solutions are shown in Figure 4. The figure includes also the reference patterns reported in the JCPDS-ICDD database for NaCl, Na_2SO_4 and $Mg_2(OH)_3Cl \cdot 4H_2O$ [45].

A number of less intense but sharp reflections are observed in the three bottom diffractograms in Figure 4, which correspond to the background electrolyte NaCl (PDF 75-0306) and Na_2SO_4 (PDF 24-1132). This indicates that the number of washing steps (five times with ethanol) was insufficient to remove the background electrolyte completely, especially in those samples with high ionic strength. The noisy, featureless background underlying the

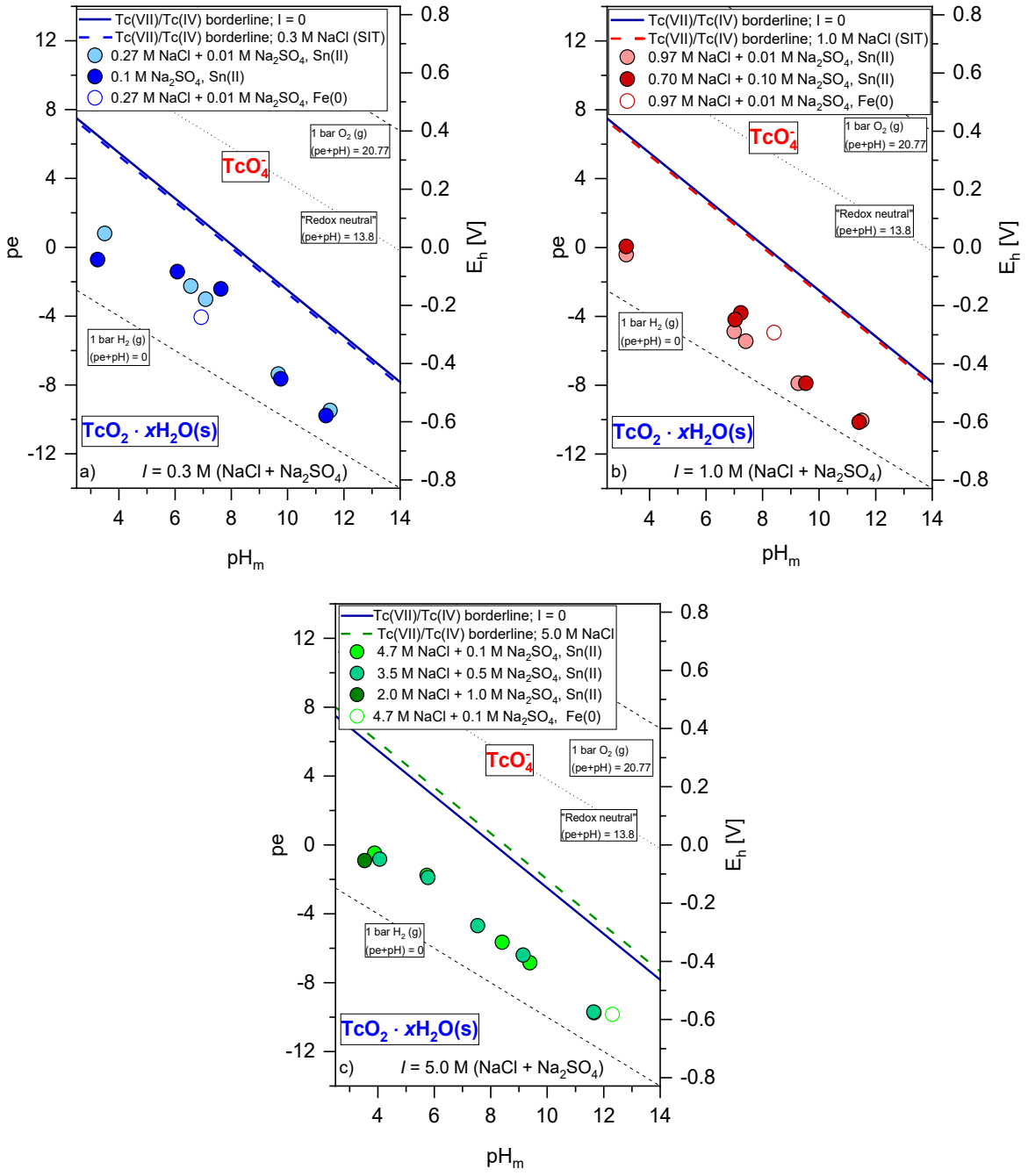

Figure 2: Experimentally measured pe and pH_m values in NaCl + Na_2SO_4 solutions with I = a) 0.3 M b) 1.0 M and c) 5.0 M. The values of pe and pH_m are plotted in Pourbaix diagrams of Tc calculated for the specific ionic strength of each system. The values were typically measured after 14–60 days sample equilibration time. Selected samples were measured up to 420 days. Solid and colored dashed lines correspond to the Tc(VII)/Tc(IV) redox borderline calculated for I = 0, 0.3 M, 1.0 and 5.0 M NaCl concentration, respectively, using thermodynamic data and SIT coefficients reported in Yalçıntaş et al. [10, 11].

reflections of NaCl and Na_2SO_4 supports the amorphous character of the Tc(IV) solid phase controlling the solubility under these conditions. The upper diffractogram in Figure 4 corresponds to a solid equilibrated in 4.1 M $MgCl_2$ + 0.3 M $MgSO_4$ at pH_m = 9.3 (pH_{max}). The featureless diffractogram points again towards an amorphous Tc(IV) solid phase. The small reflections observed can be possibly assigned to $Mg_2(OH)_3Cl{\bullet}4H_2O$(cr) (PDF 36-0388), which is the solid phase buffering the pH_m at ≈9 in concentrated $MgCl_2$ solutions.

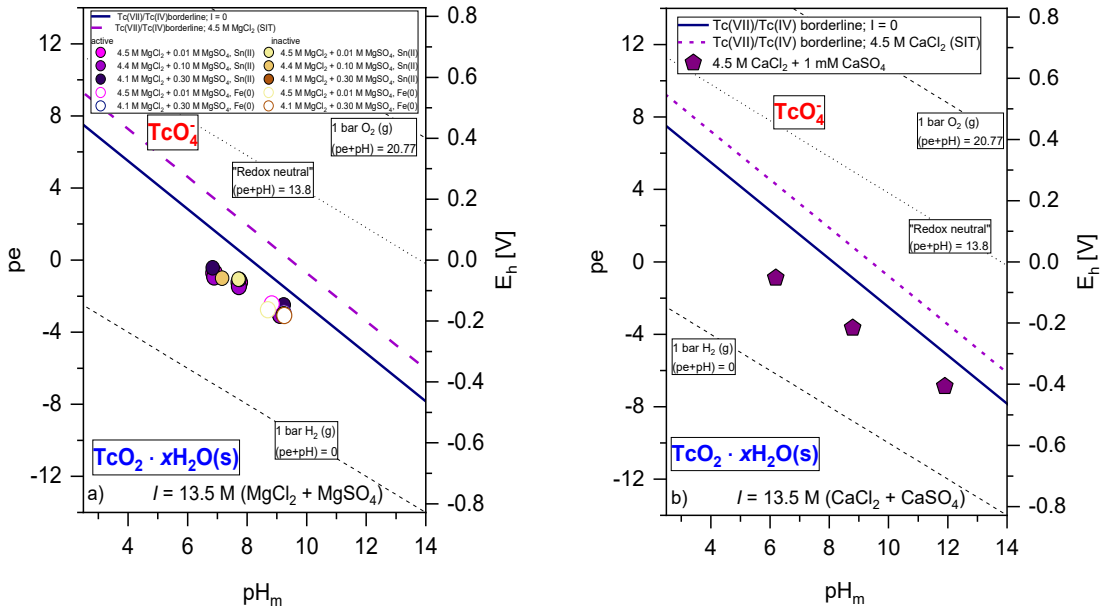

Figure 3: Experimentally measured pe and pH_m values in a) $MgCl_2$–$MgSO_4$ and b) $CaCl_2$–$CaSO_4$ solutions with I = 13.5 M. The values of pe and pH_m are plotted in Pourbaix diagrams of Tc calculated for the specific ionic strength of each system. The values were typically measured after 6–60 days sample equilibration time. Solid and colored dashed lines correspond to the Tc(VII)/Tc(IV) redox borderline calculated for I = 0 and 13.5 M $MgCl_2$ or $CaCl_2$ respectively, using thermodynamic data and SIT coefficients reported in Yalçıntaş et al. [10, 11].

Figure 5 shows a selection of SEM images obtained for Tc(IV) solid phases equilibrated in NaCl–Na_2SO_4 (pH_m = 3.5 (Figures b and c) and 11.8 (Figure a) and $MgCl_2$–$MgSO_4$ (pH_m = 9.3 (Figure d)) solutions as well as the pristine TcO_2(s) solid phase (Figure e)). Phase "1" observed in Figure 5a mostly corresponds to a Tc phase, whereas the crystalline structure "2" was identified by EDS as NaCl. The needle-like structure "3" most likely corresponds to Na_2SO_4. EDS confirms also that the amorphous aggregate in Figure 5b (found in similar shape in all investigated samples) consists mainly of Tc. Structures "2" and "3" could also be observed in Figure 5c. In spite of the rather high concentrations of sodium determined by quantitative chemical analysis, these observations support that TcO_2(am, hyd) is the solid phase controlling the solubility of Tc(IV) in the investigated samples.

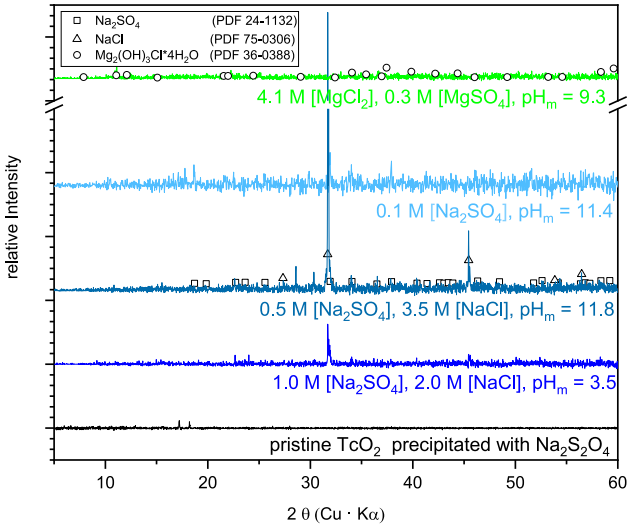

Figure 4: XRD patterns collected for Tc(IV) solid phases equilibrated in NaCl–Na_2SO_4 and $MgCl_2$–$MgSO_4$ solutions as well as the starting TcO_2(s) solid phase. Empty symbols correspond to reference patterns for NaCl, Na_2SO_4 and $Mg_2(OH)_3Cl \cdot 4H_2O$ as reported in the JCPDS-ICDD database [45].

Figure 5d shows the SEM image of the Tc solid phase equilibrated in 4.1 M $MgCl_2$ + 0.3 M $MgSO_4$ at pH_m = 9.3. EDS confirms that the large needles observed correspond to a Mg–OH–Cl phase, which was also detected by XRD. A significant content of Mg is also determined by quantitative chemical analysis, reflecting the fact that $Mg_2(OH)_3Cl \cdot 4H_2O$(cr) is present. However, EDS analysis of the amorphous material also present in this sample confirm only a very minor fraction of Mg, again supporting that the hydrous oxide TcO_2(am, hyd) is the solid phase controlling the solubility of Tc.

4.4 XANES and EXAFS measurements

The Tc K-edge XANES spectra of the selected Tc solubility samples equilibrated in solutions with I = 5.0 M

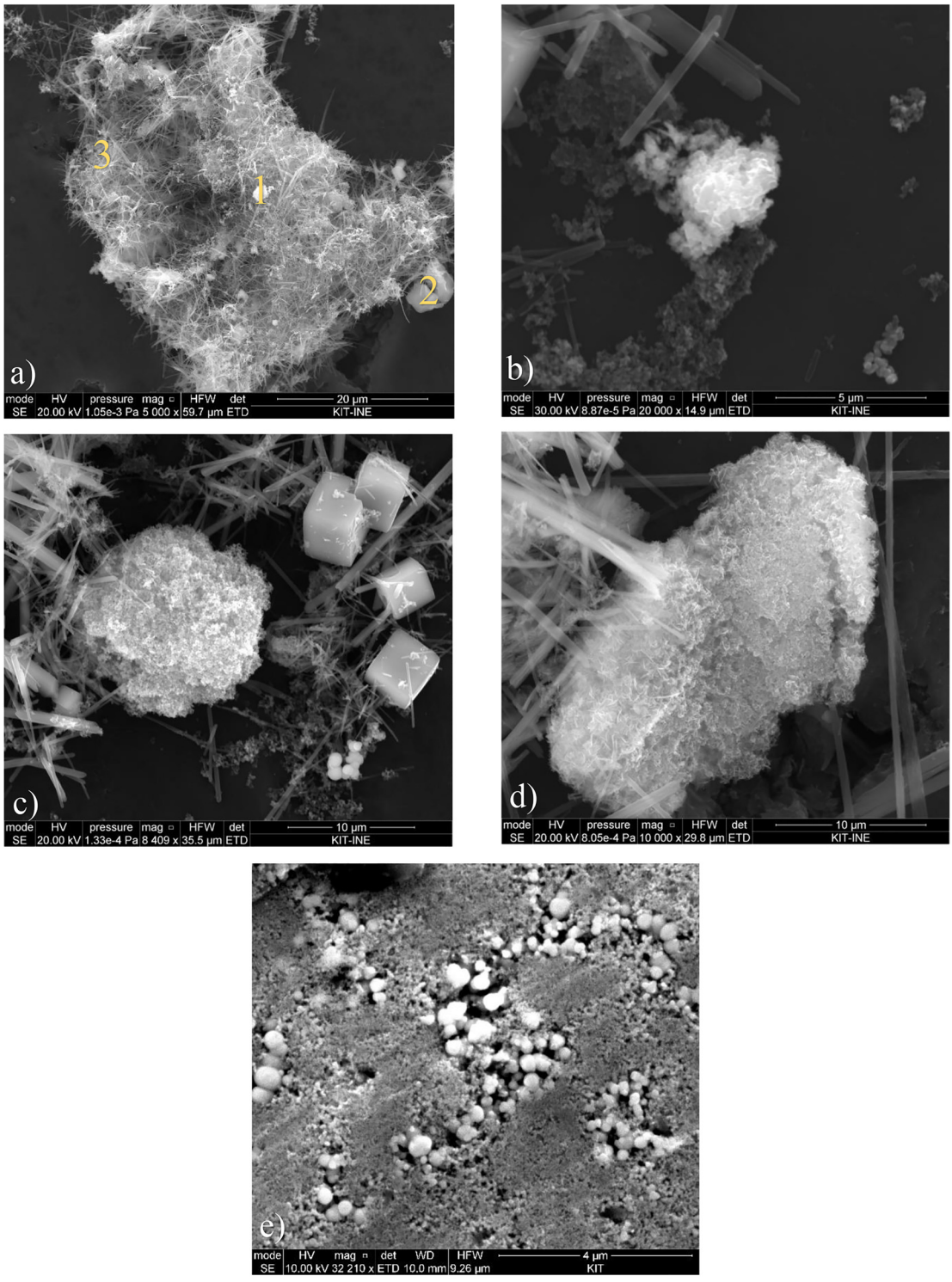

Figure 5: SEM images collected for Tc samples equilibrated in a) 3.5 M NaCl + 0.5 M Na_2SO_4, pH_m = 11.8, b) 2.0 M NaCl + 1.0 M Na_2SO_4, pH_m = 3.5, c) 2.0 M NaCl + 1.0 M Na_2SO_4, pH_m = 3.5, d) 4.1 M $MgCl_2$ + 0.3 M $MgSO_4$, pH_m = 9.3 and e) of the pristine TcO_2(s) solid phase.

NaCl + Na_2SO_4 and [Na_2SO_4] = 0.1 and 0.5 M (2 solid + 2 aqueous) are depicted in Figure 6, together with the Tc(VII) and Tc(IV) reference spectra reported in Yalçıntaş et al. [10]. Samples holding higher concentrations of Tc in the aqueous phase were chosen in order to obtain a better signal-to-noise ratio in the corresponding XANES spectra. The shape of the spectra as well as the energy positions of the inflection points of the aqueous and solid phases

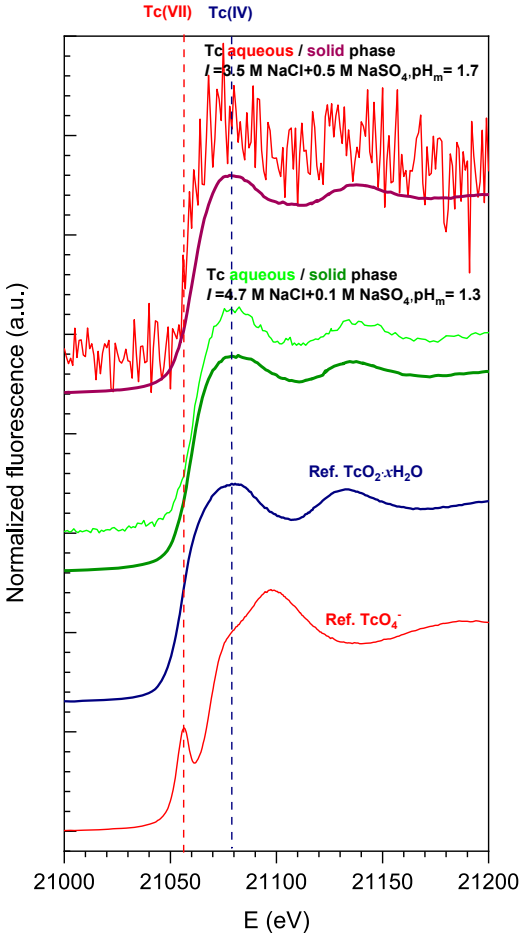

Figure 6: Tc K-edge XANES spectra of two selected solubility samples (aqueous + solid phase) equilibrated in acidic NaCl–Na_2SO_4 solutions with [Na_2SO_4] = 0.1 and 0.5 M. XANES spectra of the Tc(IV) "starting material" (solid + aqueous phase) prepared electrochemically as well as Tc(VII) and Tc(IV) references as reported in Yalçıntaş et al. appended for comparison [10].

measured clearly show the sole presence of Tc(IV) in the aqueous and solid phases of both samples, as hinted by (pe + pH_m) and solubility measurements.

The EXAFS spectra of the two solid phases in the presence of sulfate (with [Na_2SO_4] = 0.1 or 0.5 M) and their Fourier transforms are depicted in Figure 7. The structural parameters obtained in the fit are summarized in Table 5. Coordination numbers as well as Tc–O and Tc–Tc distances determined for the Tc(IV) solid phase equilibrated in 3.5 M NaCl + 0.5 M Na_2SO_4 at pH_m = 1.7 are in good agreement with data reported in the literature for TcO_2(am, hyd) [10, 46].

The fit of the EXAFS data collected from the Tc(IV) solid phase equilibrated in 4.7 M NaCl + 0.1 M Na_2SO_4 at pH_m = 1.3 requires the incorporation of an additional shell at a distance of ≈2.4 Å. Although the use of S or Cl as backscatterer results in a satisfactory fit of this shell, the predominance of a Tc(IV)–O/OH–Cl solid phase is favored considering the significantly larger Tc–S distances that would be expected in a Tc(IV)–SO_4 compound, and also in view of previous results reported in pure chloride systems. Hence, Hess and coworkers reported the formation of a Tc(IV)–O/OH–Cl solid phase at pH = 0.2 and [Cl^-] = 1.0 M with structural parameters similar to those determined in this work [47]. We note further that Tc–Cl distances in Tc(IV)Cl_4(cr) range between 2.24 and 2.50 Å, which are in line with Tc–Cl distances observed in this study [48]. Based on their solubility data, Yalçıntaş et al. suggested also the formation of a mixed Tc(IV)–O/OH–Cl solid phase in weakly acidic, concentrated $MgCl_2$ solutions [11]. As illustrated by reaction (3), the transformation of TcO_2(am, hyd) into a Tc(IV)–O/OH–Cl solid phase is favored both by increasing [H^+] and [Cl^-]:

$$TcO_2\,xH_2O\,(s) + y\,Cl^- + y\,H^+ \Leftrightarrow TcO_a\,(OH)_b Cl_y\,(x-z)H_2O\,(s) \quad (3)$$

The experimentally measured data are depicted as red lines, fits are shown as blue or dark green lines with circles/triangles. Dashed lines represent the FT windows used for the EXAFS fit.

4.5 Solubility of Tc(IV) in the presence of sulfate

4.5.1 Solubility in NaCl–$NaSO_4$ solutions

Figure 8 shows the experimental solubility data of Tc(IV) determined in solutions with I = 0.3, 1.0 and 5.0 M NaCl–Na_2SO_4 equilibrated up to $t \leq 420$ days. These results are compared to the solubility data previously reported by Yalçıntaş et al. in analogous pure NaCl solutions and absence of sulfate. The solid lines in the figures correspond to the solubility of $TcO_2{\cdot}0.6H_2O$(am) calculated for 0.3 M, 1.0 and 5.0 M NaCl solutions (absence of sulfate) using the thermodynamic and SIT activity models reported in Yalçıntaş et al. and Baumann et al. [9, 10]. The solubility results obtained in solutions with I = 0.3, 1.0 and 5.0 M NaCl–Na_2SO_4 show clear similarities. Hence, under weakly acidic to weakly alkaline conditions ($3 \leq pH_m \leq 10$), the solubility shows a pH_m-independent behavior which is in good agreement with the previously published data in pure NaCl solutions [10]. Considering a solubility control by $TcO_2{\bullet}xH_2O$(am) as hinted by solid phase characterization, the pH_m-independent behavior can be attributed to the

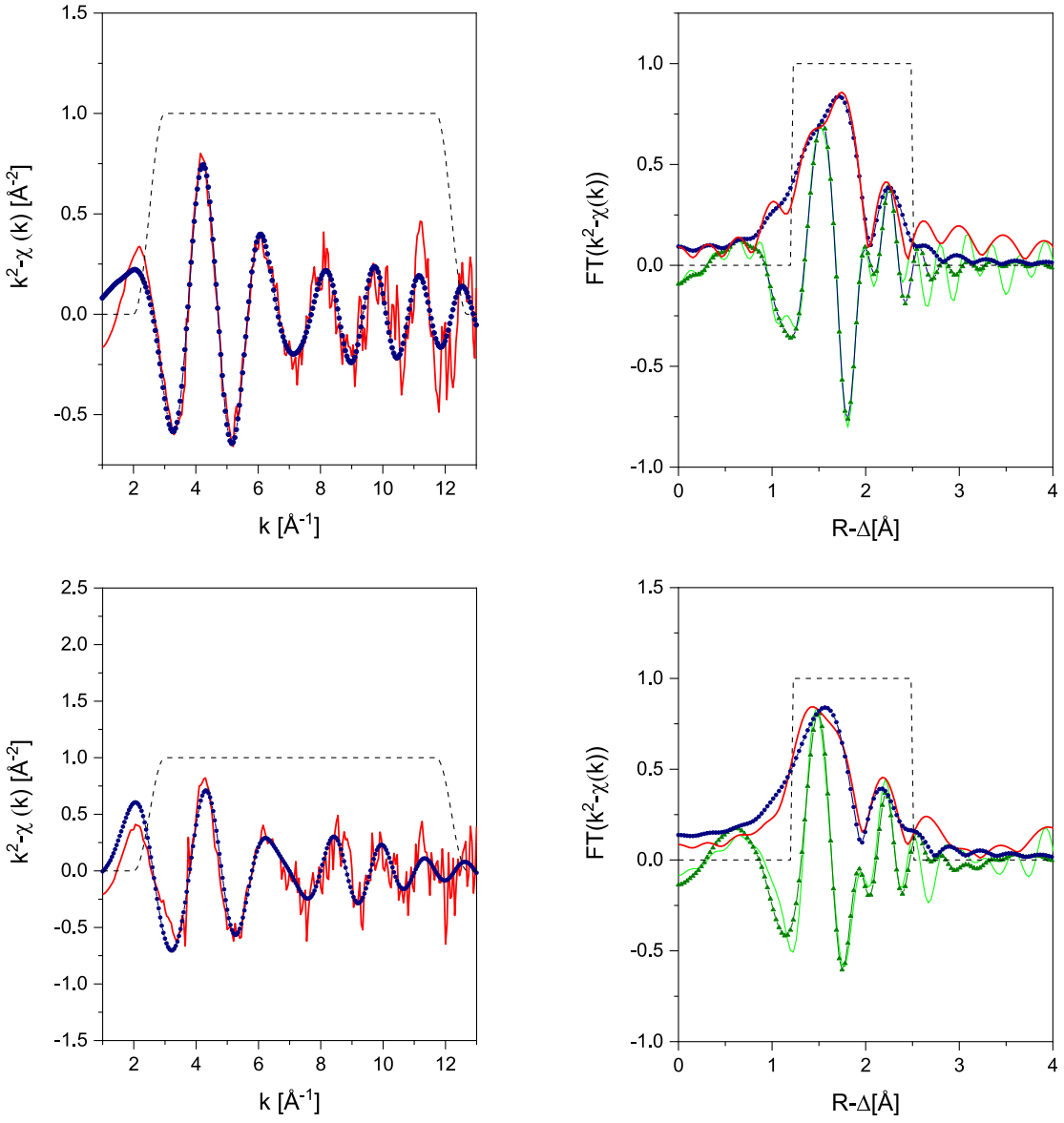

Figure 7: k^2 weighted Tc EXAFS spectra and Fourier transforms (FT) of two selected solubility samples (solid phase) equilibrated in acidic NaCl–Na_2SO_4 solutions with [Na_2SO_4] = 0.1 M (top) and [Na_2SO_4] = 0.5 M (bottom).

solubility reaction $TcO_2{\bullet}xH_2O(am) + (1 - x)\ H_2O(l) \rightleftharpoons TcO(OH)_2(aq)$. As expected for a dissolved uncharged species, the solubility is neither affected by the concentration of the background electrolyte nor by its composition, because of rather weak ion interaction processes. The slight scattering of the solubility data obtained for this pH region is also typical for such low metal concentrations in combination with the presence of a neutral species.

Under hyperalkaline conditions ($pH_m \geq 11$), the solubility of Tc(IV) increases consistently with pH, matching previous solubility data reported for pure NaCl solutions [10]. This observation is in line with the predominance of the anionic hydrolysis species $TcO(OH)_3^-$ as selected in the NEA-TDB [12, 14]. Pure Na_2SO_4 solutions show similar solubility results compared to mixed NaCl–Na_2SO_4 systems of the same ionic strength, and agree well with the calculated solubility of Tc(IV) in pure NaCl solutions.

A steep increase in the solubility can be observed in the acidic pH region ($pH_m \leq 5$) for the systems I = 1.0 and 5.0 M NaCl–Na_2SO_4, which hints (in the absence of sulfate) towards the predominance of cationic hydrolysis species. The chemical model previously selected in the NEA–TDB included the predominance of TcO^{2+} and $TcOOH^+$ species in this pH region [12]. This model was later updated by

Table 5: Structural parameters derived from EXAFS analysis for the two solid phases equilibrated in sulfate solutions.

Sample	Scattering Path	Coordination Number	Distance R (Å)	Debye Waller Parameter σ^2 (Å^2)	ΔE_0 (eV)
Tc(IV) solid phase in 3.5 M NaCl + 0.5 M $NaSO_4$	Tc–O	6.0	2.11	0.010	0.4
pH_m = 1.7	Tc–Tc	1.0[a]	2.62	0.005	
Tc(IV) solid phase in 4.7 M NaCl + 0.1 M $NaSO_4$ pH_m = 1.3	Tc–O	3.3	2.11	0.013	−6.0
	Tc–Cl	2.9	2.35	0.010	
	Tc–Tc	1.0[a]	2.63	0.004	
TcO_2 solid phase in	Tc–O	6.7	2.07	0.01	−5.15
Yalçıntaş et al. [10]	Tc–Tc	1.0[a]	2.59	0.002	
Tc solid,	Tc–O_1	4.6 ± 1.1	2.07 ± 0.02	0.10 ± 0.02	5.3 ± 2.7
pH = 1.6 [Cl] = 5 M	Tc–O_2	1.8 ± 0.5	2.71 ± 0.02	0.00 ± 0.00	6.2 ± 2.9
Hess et al. [47]	Tc–Tc	1.0 ± 0.3	2.59 ± 0.2	0.09 ± 0.01	−9.4 ± 4.2
Tc solid,	Tc–O_1	4.3 ± 1.2	2.19 ± 0.04	0.15 ± 0.02	6.7 ± 2.4
pH = 0.2 [Cl] = 1 M	Tc–O_2	1.0 ± 0.3	2.66 ± 0.02	0.00 ± 0.00	2.0 ± 3.7
Hess et al. [47]	Tc–Cl	2.0 ± 0.5	2.27 ± 0.02	0.09 ± 0.01	2.5 ± 3.2

Fit errors: CN: ±20%, R: ±0.01 Å, σ^2: ±0.001 Å^2. [a]Fixed.

Yalçıntaş et al., who defined the only formation and predominance of the trimeric species $Tc_3O_5^{2+}$ [10, 12]. Note that the recent NEA-TDB Update book favored the selection of the dimer $Tc_2O_2(OH)_2^{2+}$ instead of the trimeric species proposed by Yalçıntaş and co-workers [14]. Solubility data obtained in the present work in solutions with I = 5.0 M NaCl–Na_2SO_4, $pH_m \approx 4$ and 0.1 M ≤ [Na_2SO_4] ≤ 1.0 M are in moderate agreement with experimental data previously reported in pure NaCl systems of the same ionic strength [10]. This supports that in case Tc(IV)-sulfate complexes are forming, these are weak and do not induce any significant increase in the solubility at this pH_m. Solubility samples in very acidic conditions ($0 \le pH_m \le 2$) show slow kinetics, and it appears evident that equilibrium conditions were not attained (especially at I = 5.0 M NaCl–Na_2SO_4) even after 428 days. A similar effect was previously reported by Yalçıntaş et al. and Hess et al. in pure chloride systems [10, 47]. The formation of Tc(IV)-sulfate complexes in very acidic conditions ($pH_m \le 1.5$, [Na_2SO_4] ≥ 0.1 M) was previously reported by Vichot et al. and Parker et al., but our results do not allow an independent confirmation of these observations [17–19].

As discussed in Section 4.1, the larger uncertainty assigned to pH_m measurements in NaCl–Na_2SO_4 systems compared to pure NaCl systems must be also acknowledged in the discussion. Hence, although a clear conclusion from the results in dilute to concentrated NaCl–Na_2SO_4 systems is that sulfate has no significant impact on the solubility of Tc(IV) in weakly acidic to hyperalkaline pH_m conditions, a weak sulfate complexation cannot be completely ruled out. Based on the excellent agreement with thermodynamic calculations for pure NaCl systems, these data support that $TcO_2{\bullet}xH_2O$(am) is the solid phase controlling the solubility of Tc(IV).

4.5.2 Solubility in concentrated $MgCl_2$–$MgSO_4$ and $CaCl_2$–$CaSO_4$ solutions

Figure 9 shows the solubility of Tc(IV) in concentrated $MgCl_2$–$MgSO_4$ and $CaCl_2$–$CaSO_4$ solutions with varying sulfate concentrations. In the Ca system and because of the solubility limit imposed by the precipitation of gypsum ($CaSO_4{\cdot}2H_2O$), the concentration of sulfate was restricted to 0.001 M.

Experimental solubility data in I = 13.5 M $MgCl_2$–$MgSO_4$ solutions at $pH_m \approx 6.7$ and 7.7 with [$MgSO_4$] ≤ 1.0 M are in good agreement with solubility data previously reported by Yalçıntaş et al. in pure $MgCl_2$ solutions with the same ionic strength [10]. This reflects that sulfate has no significant impact on the solubility of Tc(IV) in this pH_m-range, and further supports that $TcO_2{\bullet}xH_2O$(am) is the solid phase controlling the solubility of Tc(IV) under these conditions. Note that the solubility at $pH_m \approx 7.7$ is very low, close or at the detection limit of LSC. The chemical reaction controlling the solubility in this region can be described as $TcO_2{\bullet}0.6H_2O$(am) + 0.4 H_2O(l) ⇌ $TcO(OH)_2$(aq), the same reaction controlling the solubility in NaCl–Na_2SO_4 solutions. However, because of the strong ion interaction processes affecting charged species at these very high ionic strength conditions, the stabilization of positively charged hydrolysis species with the consequent increase in solubility occurs at $pH_m \le 7$, in contrast with the behavior observed in dilute systems (increase in solubility only observed at $pH_m \le 3$, see Figure 8). Under more alkaline conditions ($pH_m \ge 8.5$) the solubility increases by about one order of magnitude compared to the solubility at $pH_m \approx 7.7$. Yalçıntaş et al. observed an even higher increase in solubility under analogous pH_m-

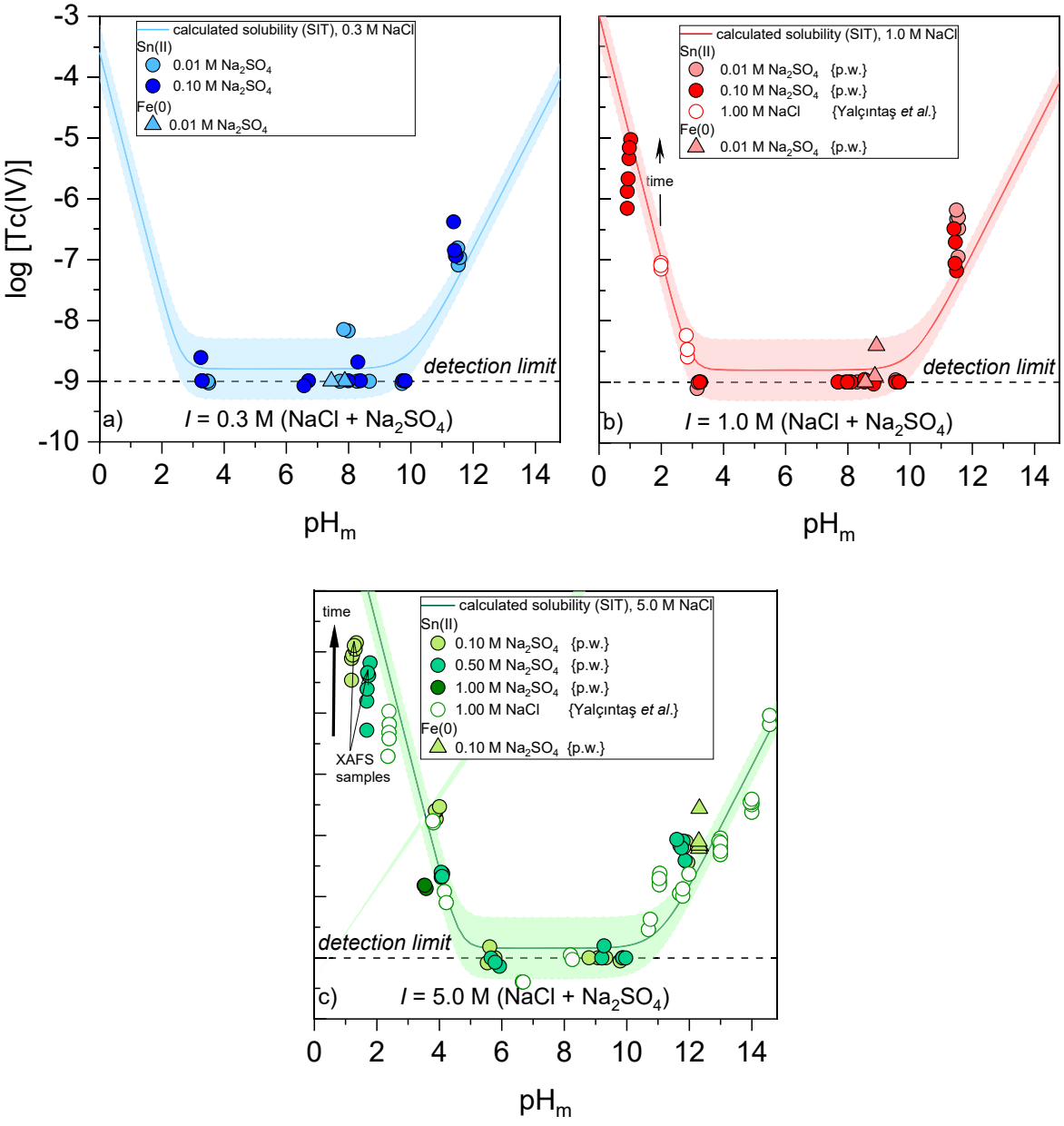

Figure 8: Experimental solubility data of Tc(IV) in NaCl–Na_2SO_4 solutions with I = a) 0.3 M, b) 1.0 M and c) 5.0 M, and 0.01 M ≤ [Na_2SO_4] ≤ 1.0 M. Tc(IV) solubility data reported by Yalçıntaş et al. under analogous conditions but absence of sulfate are appended for comparison purposes [10]. Values were typically measured after 10–52 days sample equilibration time. Selected samples were measured up to 420 days after sample equilibration. Solid lines and colored areas correspond to the solubility of TcO_2•0.6H_2O(am) calculated using thermodynamic and activity models reported in Yalçıntaş et al. and Baumann et al. [9, 10].

conditions but in the absence of sulfate, which the authors attributed to the formation of a previously unreported ternary species $Mg_3[TcO(OH)_5]^{3+}$ [10]. Solid phase characterization (XRD, see Section 4.4) of the sample at $pH_m \approx 9.3$ with 4.1 M $MgCl_2$ + 0.3 M $MgSO_4$ only showed minor reflections corresponding to $Mg_2(OH)_3Cl{\cdot}4H_2O$(cr), thus suggesting that no Tc solid phase transformation (at least resulting in a crystalline solid phase) took place under these conditions.

Assessing the impact of sulfate on the solubility of Tc(IV) in concentrated $MgCl_2$ brines is a relevant input in the context of underground repositories in salt-rock formations where significant sulfate concentration may arise in certain scenarios. Results obtained in this study provide a sound experimental evidence for the estimation of Tc(IV) solubility upper limits, hence supporting that such sulfate concentrations up to 1.0 M will not result in an increase of [Tc] compared to sulfate-free solutions.

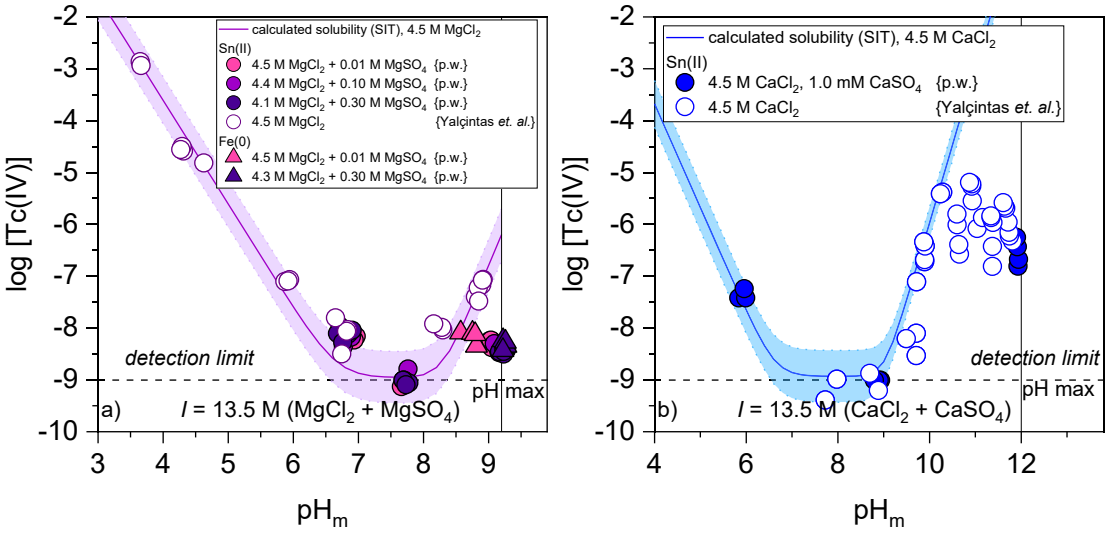

Figure 9: Experimental solubility data of Tc(IV) in a) $MgCl_2$–$MgSO_4$ and b) $CaCl_2$–$CaSO_4$ solutions with I = 13.5 M as determined in the present work. Tc(IV) solubility data reported by Yalçıntaş et al. under analogous conditions but absence of sulfate are appended for comparison purposes [10]. Values were typically measured after 7–62 days sample equilibration time. Solid lines and colored areas correspond to the solubility of TcO_2•0.6H_2O(am) calculated using thermodynamic and activity models reported in Yalçıntaş et al. [10].

The solubility of Tc(IV) in concentrated $CaCl_2$–$CaSO_4$ solutions with [$CaSO_4$] = 0.001 M at $pH_m \approx 6$ and 9 is in excellent agreement with thermodynamic calculations conducted for sulfate-free solutions of analogous ionic strength (see Figure 9). This observation reflects that the sulfate concentration considered in the present work has no impact on the solubility of Tc(IV) in this pH_m-range. On the other hand, the solubility of Tc(IV) in hyperalkaline solutions ($pH_m \approx 12$) is significantly lower than the solubility calculated using thermodynamic data reported in Yalçıntaş et al., which foresees the formation of the ternary complex $Ca_3[TcO(OH)_5]^{3+}$ [10]. These results likely reflect that thermodynamic equilibrium has not yet been attained for these samples (see Figure SM-2 in the SI). Indeed, slow kinetics at $pH_m \geq 10.5$ were also reported in Yalçıntaş et al., where equilibrium conditions were not attained even after 500 days (see empty circles in Figure 9).

5 Summary and conclusions

The solubility of Tc(IV) was investigated from undersaturation conditions in dilute to concentrated NaCl–Na_2SO_4 solutions, as well as in concentrated $MgCl_2$–$MgSO_4$ and $CaCl_2$–$CaSO_4$ solutions. Experiments were performed from acidic to hyperalkaline pH conditions under Ar atmosphere at T = (22 ± 2) °C. Very reducing conditions (with $pe + pH_m \leq 5$) were set by either Sn(II) or Fe(0) in order to stabilize technetium in its +IV oxidation state. Solid phases of selected solubility samples were characterized by XRD, SEM–EDS and XAFS measurements.

Correction factors (A_m values) required for the determination of pH_m from the experimentally measured pH_{exp} were quantified for Na_2SO_4 and mixed NaCl–Na_2SO_4 solutions. In contrast to other 1:1 and 1:2 chloride salts reported in literature, A_m values determined in this work for sulfate-containing systems are significantly lower (or even negative in the case of pure sulfate systems) and show a different, non-linear behavior with increasing salt concentration.

Redox measurements conducted in sulfate-containing solutions are in agreement with data previously reported by Yalçıntaş et al. for chloride systems in the presence of Sn(II) or Fe(0) [10, 11]. The combination of experimentally measured ($pe + pH_m$) values and thermodynamic calculations in the form of *Pourbaix* diagrams indicates the predominance of Tc(IV) in all investigated systems. Solubility data collected in sulfate-containing systems are generally in good agreement with previous solubility studies conducted in sulfate-free NaCl, $MgCl_2$ and $CaCl_2$ solutions of analogous ionic strength. This supports that sulfate has no significant impact on the solubility of Tc(IV) and the models for sulfate free solutions provided in [10] can be used in Tc(IV) solubility calculation for sulfate containing solutions.

The combination of solubility data and solid phase characterization (XRD, SEM-EDS, XANES and EXAFS) strongly support that $TcO_2 \cdot xH_2O$(am) is the solid phase controlling the solubility of Tc in the investigated systems.

Under very acidic pH conditions the formation of ternary Tc–O–Cl or mixtures of Tc–Cl and TcO_2 have been reported by Hess et al. Our EXAFS evaluation suggests also the formation of a Tc–O/OH–Cl solid phase in highly acidic HCl–NaCl solutions at pH = 1.3 similar to the results from Hess et al.

However, all other samples in this study are characterized by more alkaline pH values for which no evidence of formation of a ternary Tc–Cl species could be obtained.

This work provides a fundamental understanding of the aquatic chemistry of Tc in reducing, dilute to concentrated salt systems containing sulfate. The results obtained also provide a sound experimental evidence of the limited impact of sulfate on the solubility of Tc(IV). This applies to dilute solutions as those expected in granite- and clay-based repositories, but also to concentrated NaCl and $MgCl_2$ brines with relatively high sulfate concentrations as those eventually to be considered in potential salt-based repositories.

Acknowledgements: The authors would like to thank D. Fellhauer (KIT-INE) for the support in the Pitzer calculations. S. Kraft (KIT-INE) is kindly acknowledged for conducting ICP-OES measurements.

Author contributions: All the authors have accepted responsibility for the entire content of this submitted manuscript and approved submission.

Research funding: This work was funded by the German Federal Ministry of Economics and Technology (BMWi) within the framework of the VESPA II project under the contract number 02 E 11607C.

Conflict of interest statement: The authors declare no conflicts of interest regarding this article.

References

1. Kienzler B., Vejmelka P., Herbert H.-J., Meyer H., Altenhein-Haese C. Long-term leaching experiments of full-scale cemented waste forms: experiments and modeling. *Nucl. Technol.* 2000, *129*, 101.
2. Metz V., Geckeis H., González-Robles E., Loida A., Bube C., Kienzler B. Radionuclide behaviour in the near-field of a geological repository for spent nuclear fuel. *Radiochim. Acta* 2012, *100*, 699.
3. Fanghänel T., Könnecke T., Weger H., Paviet-Hartmann P., Neck V., Kim J. I. Thermodynamics of Cm(III) in concentrated salt solutions: carbonate complexation in NaCl solution at 25 °C. *J. Solut. Chem.* 1999, *28*, 447.
4. Lucchini J. F., Borkowski M., Richmann M. K., Reed D. T. Uranium(VI) solubility in carbonate-free WIPP brine. *Radiochim. Acta Int. J. Chem. Asp. Nucl. Sci. Technol.* 2013, *101*, 391.
5. Wieland E., Van Loon L. R. *Cementitious Near-Field Sorption Data Base for Performance Assessment of an ILW Repository in Opalinus Clay*; Paul Scherrer Institute: CH-5232 Villigen PSI ,Switzerland, 2003.
6. Eriksen T. E., Ndalamba P., Bruno J., Caceci M. The solubility of $TcO_2 \cdot nH_2O$ in neutral to alkaline solutions under constant p_{CO2}. *Radiochim. Acta* 1992, *58–59*, 67.
7. Eriksen T. E., Ndalamba P., Cui D., Bruno J., Caceci M., Spahiu K. Solubility of the redox-sensitive radionuclides ^{99}Tc and ^{237}Np under reducing conditions in neutral to alkaline solutions. Effect of carbonate. *SKB Tech. Rep.* 1993, *93–18*, 41.
8. Baumann A., Yalçıntaş E., Gaona X., Polly R., Dardenne K., Prüßmann T., Rothe J., Altmaier M., Geckeis H. Thermodynamic description of Tc(IV) solubility and carbonate complexation in alkaline $NaHCO_3$–Na_2CO_3–NaCl systems. *Dalton Trans.* 2018, *47*, 4377.
9. Baumann A., Yalçıntaş E., Gaona X., Altmaier M., Geckeis H. Solubility and hydrolysis of Tc(IV) in dilute to concentrated KCl solutions: an extended thermodynamic model for Tc^{4+}–H^+–K^+–Na^+–Mg^{2+}–Ca^{2+}–OH^-–Cl^-–H_2O(l) mixed systems. *New J. Chem.* 2017, *41*, 9077.
10. Yalçıntaş E., Gaona X., Altmaier M., Dardenne K., Polly R., Geckeis H. Thermodynamic description of Tc(IV) solubility and hydrolysis in dilute to concentrated NaCl, $MgCl_2$ and $CaCl_2$ solutions. *Dalton Trans.* 2016, *45*, 8916.
11. Yalçıntaş E., Gaona X., Scheinost A. C., Kobayashi T., Altmaier M., Geckeis H. Redox chemistry of Tc(VII)/Tc(IV) in dilute to concentrated NaCl and $MgCl_2$ solutions. *Radiochim. Acta* 2015, *103*, 57.
12. Guillaumont R., Fanghänel T., Fuger J., Neck V., Palmer D. A., Grenthe I., Rand M. H. *Update on the Chemical Thermodynamics of Uranium, Neptunium, Plutonium, Americium and Technetium, Vol. 5 of Chemical Thermodynamics*; Elsevier: North-Holland, Amsterdam, 2003.
13. Rard J. A., Anderegg G., Wanner H., Rand M. H. In *Chemical Thermodynamics of Technetium*; OECD Nuclear Agency Data Bank, Ed. North Holland Elsevier Science Publishers B.V.: Amsterdam, The Netherlands, 1999 Chapter III, pp. 37–44; and Chapter V, pp. 63–26.
14. Grenthe I., Gaona X., Plyasunov A. V., Linfeng R., Runde W. H., Grambow B., Konings R. J. M., *Second Update on the Chemical Thermodynamics of U, Np, Pu, Am and Tc*; OECD Publications: Paris; France, 2020.
15. Spitsyn V. I., Kuzina A. F., Oblova A. A., Glinkina M. I., Stepovaya L. I. On the mechanism of the electrochemical reduction of TcO_4^{-1} ion on platinum cathode in sulphuric acid solutions. *J. Radioanal. Chem.* 1976, *30*, 561.
16. Ianovici E., Kosinski M., Lerch P., Maddock A. G. The aquation of hexachlorotechnetate(IV). *J. Radioanal. Nucl. Chem.* 1981, *64*, 315.
17. Vichot L., Ouvrard G., Montavon G., Fattahi M., Musikas C., Grambow B. XAS study of technetium(IV) polymer formation in mixed sulphate/chloride media. *Radiochim. Acta* 2002, *90*, 575.
18. Vichot L., Fattahi M., Musikas C., Grambow B. Tc(IV) chemistry in mixed chloride/sulphate acidic media. Formation of polyoxopolymetallic species. *Radiochim. Acta* 2003, *91*, 263.
19. Parker T. G., Omoto T., Dickens S. M., Wall D. E., Wall N. A. Complexation of Tc(IV) with SO_4^{2-} in NaCl medium. *J. Solut. Chem.* 2018, *47*, 1192.
20. Altmaier M., Gaona X., Fanghänel T. Recent advances in aqueous actinide chemistry and thermodynamics. *Chem. Rev.* 2013, *113*, 901.

21. Neck V., Kim J. I. Solubility and hydrolysis of tetravalent actinides. *Radiochim. Acta* 2001, *89*, 1.
22. Shannon R. D. Revised effective ionic radii and systematic studies of interatomic distances in halides and chalcogenides. *Acta Crystallogr. A* 1976, *32*, 751.
23. Rand M. H., Fuger J., Grenthe I., Neck V., Rai D. *Chemical Thermodynamics of Thorium*; OECD Nuclear Agency Data Bank, Ed.; OECD Publications: Paris, France, 2008; p. 161f.
24. Brown P. L., Curti E., Grambow B., Ekberg C. *Chemical Thermodynamics of Zirconium*; OECD Nuclear Energy Agency Data Bank, Ed.; North Holland Elsevier Science Publishers B.V.: Amsterdam, The Netherlands, 2005; pp. 101–191.
25. Gaona X., Fellhauer D., Altmaier M. Thermodynamic description of Np(VI) solubility, hydrolysis, and redox behavior in dilute to concentrated alkaline NaCl solutions. *Pure Appl. Chem.* 2013, *85*, 2027.
26. Altmaier M., Metz V., Neck V., Müller R., Fanghänel T. Solid-liquid equilibria of $Mg(OH)_2$(cr) and $Mg_2(OH)_3Cl{\cdot}4H_2O$(cr) in the system Mg–Na–H–OH–Cl–H_2O at 25 °C. *Geochem. Cosmochim. Acta* 2003, *67*, 3595.
27. Altmaier M., Neck V., Fanghänel T. Solubility of Zr(IV), Th(IV) and Pu(IV) hydrous oxides in $CaCl_2$ solutions and the formation of ternary Ca–M(IV)–OH complexes. *Radiochim. Acta* 2008, *96*, 541–550.
28. Herm M., Gaona X., Rabung T., Fellhauer D., Crepin C., Dardenne K., Altmaier M., Geckeis H. Solubility and spectroscopic study of AnIII/LnIII in dilute to concentrated Na–Mg–Ca–Cl–NO_3 solutions. *Pure Appl. Chem.* 2015, *87*, 487.
29. Rai D., Felmy A. R., Juracich S. P., Rao F. *Estimating the Hydrogen Ion Concentration in Concentrated NaCl and Na_2SO_4 Electrolytes. Sandia National Labs., Albuquerque, NM (United States)*; Pacific Northwest Lab.: Richland, WA (United States), 1995.
30. Moog H. C., Bok F., Marquardt C. M., Brendler V. Disposal of nuclear waste in host rock formations featuring high-saline solutions – implementation of a thermodynamic reference database (THEREDA). *Appl. Geochem.* 2015, *55*, 72.
31. Altmaier M., Brendler V., Hagemann S., Herbert H.-J., Kienzler B., Marquardt C. M., Moog H. C., Neck V., Richter A., Voigt W., Wilhelm S. THEREDA – Ein Beitrag zur Langzeitsicherheit von Endlagern nuklearer und nichtnuklearer Abfälle. *ATW – Int. J. Nucl. Power* 2008, *4*, 13f.
32. Parkhurst D. L., Appelo C. A. J. Description of Input and Examples for PHREEQC Version 3—a Computer Program for Speciation, Batch-Reaction, One-Dimensional Transport, and Inverse Geochemical Calculations, In *US Geological Survey Techniques and Methods*, book 6, chap A43, p 497, 2013, http://pubs.usgs.gov/tm/06/a43.
33. Kurnaow N. S., Žemčužny S. F. Die Gleichgewichte des reziproken Systems Natriumchlorid-magnesiumsulfat mit Berücksichtigung der natürlichen Salzsolen. *Z. Anorg. Allg. Chem.* 1924, *140*, 149.
34. Li Z., Demopoulos G. P. Solubility of $CaSO_4$ phases in aqueous HCl + $CaCl_2$ solutions from 283 to 353 K. *J. Chem. Eng. Data* 2005, *50*, 1971.
35. Kobayashi T., Scheinost A. C., Fellhauer D., Gaona X., Altmaier M. Redox behavior of Tc(VII)/Tc(IV) under various reducing conditions in 0.1 M NaCl solutions. *Radiochim. Acta* 2013, *101*, 323.
36. Gamsjäger H., Gajda T., Sangster J., Saxena S. K., Voigt W. *Chemical Thermodynamics of Tin OECD Nuclear Energy Agency Data Bank*; North Holland Elsevier Science Publishers B. V.: Amsterdam, The Netherlands, 2012.
37. Altmaier M., Neck V., Fanghänel T. Solubility and colloid formation of Th(IV) in concentrated NaCl and $MgCl_2$ solution. *Radiochim. Acta* 2004, *92*, 537.
38. Wong-Ng W., McMurdie H. F., Hubbard C. R., Mighell A. D. JCPDS-ICDD research associateship (Cooperative Program with NBS/NIST). *J. Res. Natl. Inst. Stand. Technol.* 2001, *106*, 1013.
39. Zimina A., Dardenne K., Denecke M. A., Grunwaldt J. D., Huttel E., Lichtenberg H., Mangold S., Pruessmann T., Rothe J., Steininger R., Vitova T. The CAT-ACT beamline at ANKA: a new high energy X-ray spectroscopy facility for CATalysis and ACTinide research. *J. Phys. Conf. Ser.* 2016, *712*, 012019.
40. Rothe J., Butorin S., Dardenne K., Denecke M. A., Kienzler B., Löble M., Metz V., Seibert A., Steppert M., Vitova T., Walther C., Geckeis H. The INE-beamline for actinide science at ANKA. *Rev. Sci. Instrum.* 2012, *83*, 043105.
41. Vanysek P. Electrochemical series. *CRC Handb. Chem. Phys.* 2000, *8*, 5–78.
42. Lide D. R. *CRC Handbook of Chemistry and Physics: A Ready-Reference Book of Chemical and Physical Data*; CRC Press: Boca Raton, Florida, USA, 1995; p. 2648.
43. Roh Y., Lee S. Y., Elless M. P. Characterization of corrosion products in the permeable reactive barriers. *Environ. Geol.* 2000, *40*, 184.
44. Duro L., El Aamrani S., Rovira M., de Pablo J., Bruno J. Study of the interaction between U(VI) and the anoxic corrosion products of carbon steel. *Appl. Geochem.* 2008, *23*, 1094.
45. Gates-Rector S., Blanton T. The powder diffraction file: a quality materials characterization database. *Powder Diffr.* 2019, *34*, 352.
46. Lukens W. W., Bucher J. J., Edelstein N. M., Shuh D. K. Products of pertechnetate radiolysis in highly alkaline solution: structure of $TcO_2{\cdot}xH_2O$. *Environ. Sci. Technol.* 2002, *36*, 1124.
47. Hess N. J., Xia Y., Rai D., Conradson S. D. Thermodynamic model for the solubility of $TcO_2 \cdot xH_2O$(am) in the aqueous Tc(IV)–Na^+–Cl^-–H^+–OH^-–H_2O system. *J. Solut. Chem.* 2004, *33*, 199.
48. Elder M., Penfold B. R. The crystal structure of technetium (IV) chloride. A new AB4 structure. *Inorg. Chem.* 1966, *5*, 1197.

Supplementary Material: The online version of this article offers supplementary material (https://doi.org/10.1515/ract-2021-1044).